COBEM 2023 27TH INTERNATIONAL CONGRESS OF MECHANICAL ENGENEERING

ABCM Brazilian Society of Mechanical Sciences and Engineering
27th ABCM International Congress of Mechanical Engineering
December 04-08, 2023, Florianópolis-SC, Brazil

COB-2023-1797
BANDGAP ANALYSIS FOR PERIODIC FRAME METASTRUCTURE COUPLED WITH LOCAL RESONATORS

Wanderson Vinicius de Oliviera Monteiro
José Maria Campos dos Santos
University of Campinas, UNICAMP-FEM-DMC, Rua Mendeleyev 200, Cidade Universitária Zeferino Vaz, Campinas - SP, Brazil.
w203198@dac.unicamp.br, zema@fem.unicamp.br

Edilson Dantas Nóbrega
Federal University of Maranhão, UFMA-CCET-CCEM, Cidade Universitária Dom Delgado, São Luís - MA, Brazil.
edilson.dantas@ufma.br

Abstract. *Vibration control in structures is essential to guarantee the stability and safety of the people who use them. For decades, several techniques have been developed to control vibration, recently, metastructures have attracted attention for their unique properties of controlling wave propagation in structures making them of great interest for modern engineering. In this work, we investigate the use of metastructure to control vibrations in structures using the Spectral Element Method (SEM) , Finite Element Method (FEM) and Wave Finite Element (WFE) method to analyze the dynamics of metastructures. These metastructures are built with periodic unit-cells, which are made by two materials coupled with local resonators. Forced responses are calculated to determine the attenuation regions along the frame structure. The influence of the constituent properties of the structure on its formation is evaluated through band-gaps obtained. Obtained results show frequency bands where the wave propagation does not occur (bandgaps), and the structure's forced response exhibited attenuation at the same range frequency. The present study made it possible to understand the behavior of the presented structure, where the obtained results contribute to the expansion of the possibilities of application of metastructure in the control of vibrations in structures.*

Keywords: *Metastructure, Periodic structures, Wave propagation, Bandgaps, Dispersion diagram.*

1. INTRODUCTION

Since the mid-20th century, the study of the theory of elastic wave propagation in periodic structures has generated significant interest. The study of wave propagation in periodic structures was initiated by Mead (Mead, 1970). During this period, the Bragg scattering mechanism was elucidated, revealing the formation of Bragg-type forbidden bands, known as bandgaps, in the frequency range determined by Bragg conditions. In recent decades, phononic crystals (PCs), which are artificially composed periodic structures, have received renewed attention.

Phononic crystals (PCs), as acoustic metamaterials or elastic metamaterials, have gained prominence in the fields of acoustics, mechanics, materials science, and engineering. The fundamental idea behind these materials lies in their spatial periodicity, phases, internal geometry, boundary conditions, or incorporation of multimaterials, along with the addition of local resonators. These crystals are composed of a unit cell that is periodically spaced, creating a unique characteristic of a bandgap. These regions of the frequency spectrum exhibit attenuation in propagation due to the effects of Bragg scattering or local resonance (Hussein *et al.*, 2014; Nanda and Karami, 2018).

Over the years, extensive research has been conducted on a variety of periodic structures, encompassing both one-dimensional and two-dimensional structures such as periodic beams, truss structures, and plates (Goto *et al.*, 2020; Zhang *et al.*, 2019; Zuo *et al.*, 2016; Miranda Jr. and Dos Santos, 2018). These studies have focused on exploring the properties of bandgaps in relation to design parameters such as structural lengths, number of cells, structural configurations, loading conditions, and structural damping. To analyze the dynamic problems associated with periodic structures, various methods have been proposed. Among them, notable methods include the Finite Element Method (FEM), the Wave Finite Element Method (WFE), the Spectral Element Method (SEM), the Plane Wave Expansion Method (PWEM), and the Transfer Matrix Method (TM).

In this work, an investigation was conducted on the wave propagation in a periodic metastructure composed of two different materials, with the coupling of local resonators. The Finite Element Method (FEM), Spectral Element Method (SEM), and Wave Finite Element Method (WFE) were employed for vibration control, bandgap formation, and parametric variation analysis.

2. THE PROPOSED STRUCTURE AND METHODS APPLICATIONS

The simplified basic structure evaluated in this work is shown in Fig. (1), where each member is composed of three Euler-Bernoulli beams made of two distinct materials, with one resonator coupled at each junction of the beams. Each color represents a material, assuming they are elastic, homogeneous, and isotropic materials. The structure can be arranged in the form of an $m \times n$ matrix, where n represents the expansion of the structure in the x direction and m in the y direction, with the periodicity occurring in the latter direction.

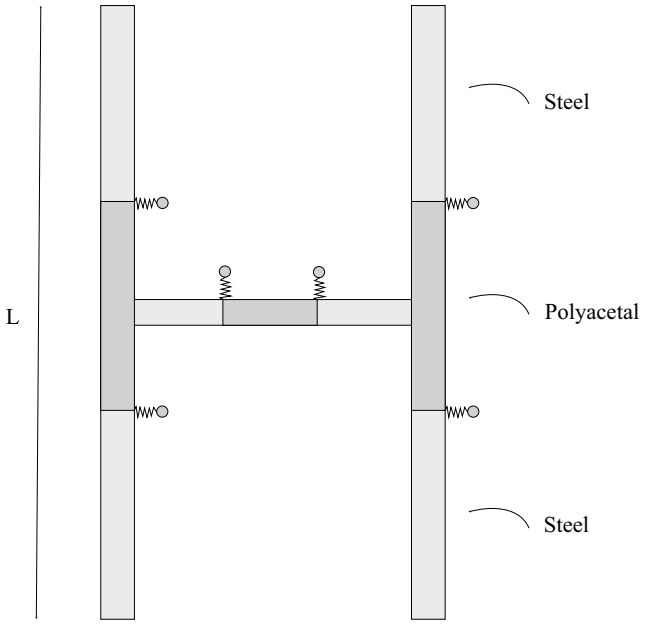

Figure 1: Simplified physical model for the 1 $\times$ 1 frame.

Figure 2 corresponds to a 1 $\times$ n arrangement of the structure, showing the analyzed boundary conditions, which are of the free-free type. A unit force with intensity F_o is applied at the beginning of the structure, and the point Q represents the end of the structure where the measurement is taken. On the other hand, Fig. 3 shows the structural periodicity of m $\times$ n, where N_c represents the number of structural cells.

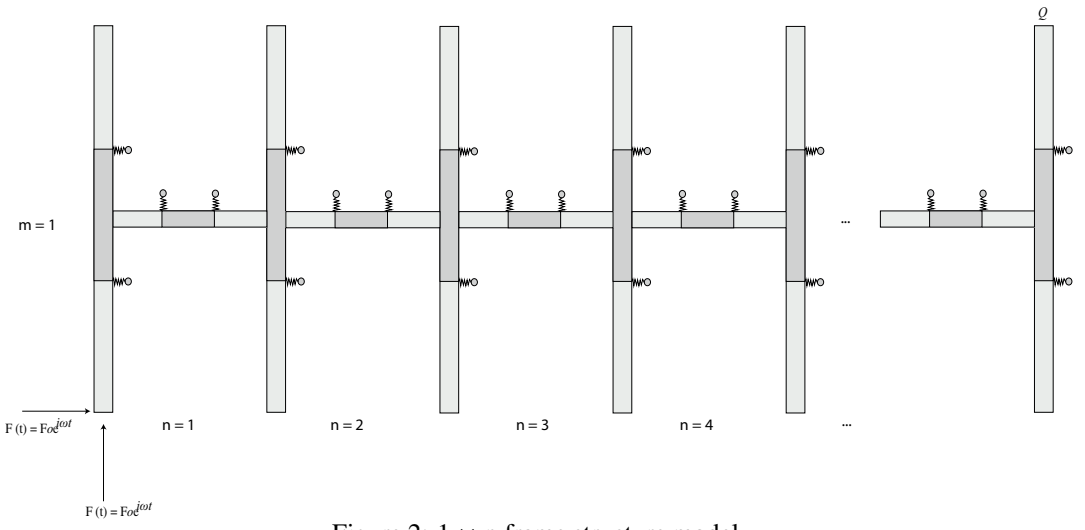

Figure 2: 1 $\times$ n frame structure model.

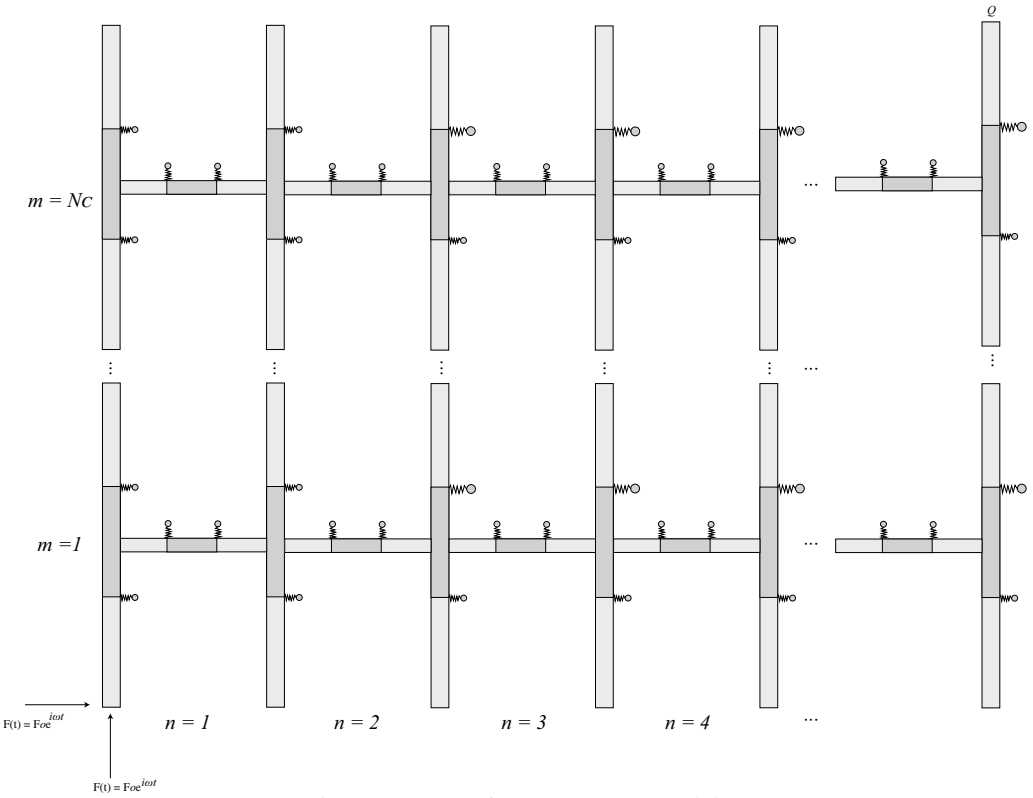

Figure 3: m $\times$ n frame structure model.

2.1 Finite Element Method in Frame Structures

Considering a planar frame, as shown in Fig. 4, which is vibrating within its own plane. Each element of the frame is capable of undergoing axial, transverse, and rotational deformations.

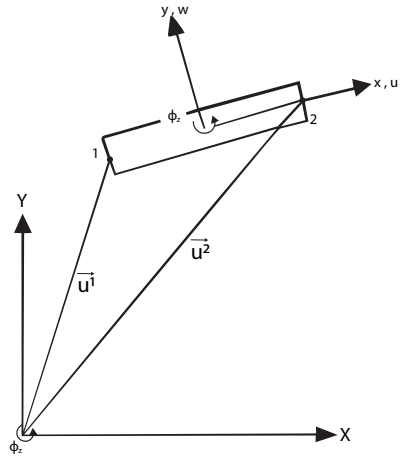

Figure 4: Geometry of a plane frame element.

From the energy expressions in each element, in terms of the degrees of freedom, the mass and stiffness matrices are obtained in the local coordinate system (M.Petyt, 2010).

$$\bar{\mathbf{k}}_e = \frac{EI_z}{2L_e^3}\begin{bmatrix} (L_e/r_z)^2 & 0 & 0 & -(L_e/r_z)^2 & 0 & 0 \\ 0 & 3 & 3L_e & 0 & -3 & 3L_e \\ 0 & 3L_e & 4L_e^2 & 0 & -3L_e & 2L_e^2 \\ -(L_e/r_z)^2 & 0 & 0 & (L_e/r_z)^2 & 0 & 0 \\ 0 & -3 & -3L_e & 0 & 3 & -3L_e \\ 0 & 3L_e & 2L_e^2 & 0 & -3L_e & 4L_e^2 \end{bmatrix} \tag{1}$$

$$\bar{\mathbf{m}}_e = \frac{\rho A L_e}{105}\begin{bmatrix} 70 & 0 & 0 & 35 & 0 & 0 \\ 0 & 78 & 22L_e & 0 & 27 & -13L_e \\ 0 & 22L_e & 8L_e^2 & 0 & -13L_e & -6L_e^2 \\ 35 & 0 & 0 & 70 & 0 & 0 \\ 0 & 27 & 13L_e & 0 & 78 & -22L_e \\ 0 & -13L_e & -6L_e^2 & 0 & -22L_e & 8L_e^2 \end{bmatrix} \tag{2}$$

Where $r_z^2 = I_z/A$ represents the radius of gyration of the cross-sectional area about the z-axis, where I_z is the moment of inertia of the Euler-Bernoulli beam and A is the cross-sectional area. L_e is half the length of each element, and ρ is the density of the material composing the beam (M.Petyt, 2010). For the structure shown in Fig.3 and Fig. 2, it is necessary to perform the transformation from the local coordinate system to the global coordinate system using the local-to-global coordinate transformation matrix ($\mathbf{\Psi}$).

$$\mathbf{\Psi} = \begin{bmatrix} \cos(\theta) & -\sin(\theta) & 0 & 0 & 0 & 0 \\ \sin(\theta) & \cos(\theta) & 0 & 0 & 0 & 0 \\ 0 & 0 & 1 & 0 & 0 & 0 \\ 0 & 0 & 0 & \cos(\theta) & -\sin(\theta) & 0 \\ 0 & 0 & 0 & \sin(\theta) & \cos(\theta) & 0 \\ 0 & 0 & 0 & 0 & 0 & 1 \end{bmatrix} \tag{3}$$

Considering θ as the rotation angle in the local coordinate system, measured counterclockwise, the global stiffness matrix ($\mathbf{K}$) and global mass matrix ($\mathbf{M}$) can be obtained through the local-to-global coordinate transformation matrix ($\mathbf{\Psi}$).

$$\begin{aligned} \mathbf{K} &= \mathbf{\Psi}^T \bar{\mathbf{k}}_\mathbf{e} \mathbf{\Psi} \\ \mathbf{M} &= \mathbf{\Psi}^T \bar{\mathbf{m}}_\mathbf{e} \mathbf{\Psi} \end{aligned} \tag{4}$$

The dynamic analysis of the structure is obtained from the dynamic stiffness matrix ($\mathbf{D}$), as follows:

$$\mathbf{D}(\omega) = \mathbf{K} - \omega^2 \mathbf{M} \tag{5}$$

Where ω is the angular frequency, the displacements are obtained from the equation of dynamic equilibrium:

$$\mathbf{D}(\omega)\mathbf{u} = \mathbf{F} \tag{6}$$

Where,

$$\begin{aligned} \mathbf{u} &= \begin{bmatrix} u_1 & w_1 & \phi_1 & u_2 & w_2 & \phi_2 & \dots & u_J & w_J & \phi_J \end{bmatrix}^T \\ \mathbf{F} &= \begin{bmatrix} N_1 & V_1 & M_1 & N_2 & V_2 & M_2 & \dots & N_J & V_J & M_J \end{bmatrix}^T \end{aligned} \tag{7}$$

Where $\mathbf{u}$ is the vector of degrees of freedom and $\mathbf{F}$ is the vector of nodal forces, with J being the total number of nodes in the structure. u_i, w_i, and ϕ_i ($i = 1, 2, \dots J$) are the nodal components of axial displacement, transverse displacement, and rotation, respectively. N_i, V_i, and M_i ($i = 1, 2, \dots J$) are the nodal components of axial force, transverse shear force, and bending moments, respectively.

The dynamic stiffness matrix of the local resonator in a spring-mass absorber system on a beam was derived by (Xiao *et al.*, 2013).

$$\mathbf{D_r} = \begin{bmatrix} \mathbf{0} & \mathbf{0} & \mathbf{0} \\ \mathbf{0} & D_0 & \mathbf{0} \\ \mathbf{0} & \mathbf{0} & \mathbf{0} \end{bmatrix}, \qquad D_0 = -\left(\omega^2 m_r + \frac{\omega^2 k_r m_r}{k_r - \omega^2 m_r}\right), \qquad f_r = \frac{1}{2\pi}\sqrt{\frac{k_r}{m_r}} \tag{8}$$

Where k_r and m_r are the effective stiffness and effective mass of the resonator, and f_r is the resonance frequency of the spring-mass absorber system. For the proposed structure, the resonators were added to the transverse degree of freedom at the junction of the materials, resulting in the summation of the dynamic stiffness matrix of the structure from Eq. (5).

2.2 Wave Finite Element Method

Developed by Mencik (2008), the method utilizes a wave propagation approach in a periodic structure. Starting from the matrices in Eq.(5) of the structure in Fig.2, the structure is separated into inner degrees of freedom $()_i$, left $()_l$, and right $()_r$.

$$\begin{bmatrix} \mathbf{D_{ii}} & \mathbf{D_{il}} & \mathbf{D_{ir}} \\ \mathbf{D_{li}} & \mathbf{D_{ll}} & \mathbf{D_{lr}} \\ \mathbf{D_{ri}} & \mathbf{D_{rl}} & \mathbf{D_{rr}} \end{bmatrix} \begin{Bmatrix} \mathbf{u_i} \\ \mathbf{u_l} \\ \mathbf{u_r} \end{Bmatrix} = \begin{Bmatrix} \mathbf{0_i} \\ \mathbf{F_l} \\ \mathbf{F_r} \end{Bmatrix} \tag{9}$$

In which its order is reduced, known as the condensed stiffness matrix:

$$\begin{bmatrix} \mathbf{D_{ll}} & \mathbf{D_{lr}} \\ \mathbf{D_{rl}} & \mathbf{D_{rr}} \end{bmatrix} \begin{Bmatrix} \mathbf{u_l} \\ \mathbf{u_r} \end{Bmatrix} = \begin{Bmatrix} \mathbf{F_l} \\ \mathbf{F_r} \end{Bmatrix} \tag{10}$$

Where $\mathbf{D_{ll}}$ = $\mathbf{D_{ll}}$ - $\mathbf{D_{li}}\mathbf{D_{ii}^{-1}}\mathbf{D_{il}}$, $\mathbf{D_{rl}}$ = $\mathbf{D_{rl}}$ - $\mathbf{D_{ri}}\mathbf{D_{ii}^{-1}}\mathbf{D_{il}}$, $\mathbf{D_{lr}}$ = $\mathbf{D_{lr}}$ - $\mathbf{D_{li}}\mathbf{D_{ii}^{-1}}\mathbf{D_{ir}}$ e $\mathbf{D_{rr}}$ = $\mathbf{D_{rr}}$ - $\mathbf{D_{ri}}\mathbf{D_{ii}^{-1}}\mathbf{D_{ir}}$. Rewriting the matrix from Eq. (10) in terms of a single generalized coordinate to avoid issues of ill-conditioning (Zhong and Williams, 1995):

$$\mathbf{q_l} = \underbrace{\begin{bmatrix} \mathbf{I_n} & 0 \\ -\mathbf{D_{ll}} & -\mathbf{D_{lr}} \end{bmatrix}}_{L_i} \underbrace{\begin{Bmatrix} \mathbf{u_l} \\ \mathbf{u_r} \end{Bmatrix}}_{\xi_i} \quad \text{and} \quad \mathbf{q_r} = \underbrace{\begin{bmatrix} 0 & \mathbf{I_n} \\ \mathbf{D_{rl}} & \mathbf{D_{rr}} \end{bmatrix}}_{N_i} \underbrace{\begin{Bmatrix} \mathbf{u_l} \\ \mathbf{u_r} \end{Bmatrix}}_{\xi_i} \tag{11}$$

where $\mathbf{q_l} = \mathbf{u_l} \ \ \mathbf{F_l}^T$ and $\mathbf{q_r} = \mathbf{u_r} \ \ \mathbf{F_r}^T$, $\mathbf{I_n}$ is the identity matrix of the same order as the degrees of freedom on the left (or right) side of the structure. Due to the periodicity of the structure, there is a relationship between consecutive cells m and $m+1$, such that $\mathbf{q_r}^m = \mathbf{q_l^{m+1}}$. Substituting this relationship into Eq. (11) and using the Floquet-Bloch theorem, we have:

$$e^{\mu}\mathbf{L_i}\xi_\mathbf{i} = \mathbf{N_i}\xi_\mathbf{i} \tag{12}$$

where $\mu = -jkL$ corresponds to propagation constant with j as imaginary number, k is the wave number , L cell length and $\mathbf{L}\xi_\mathbf{i}$ are the eigenvectors.

2.2.1 Wave mode expansion

Considering a periodic structure composed of N_c cells and $N_c + 1$ interfaces, we can express the displacement and nodal forces of each unit cell (m) as follows:

$$\begin{aligned} \mathbf{u}^{(m)} &= Q^{(m)}\mathbf{\Phi}_u\mu^{(m-1)} + Q^{\star(m)}\mathbf{\Phi}_u^\star\mu^{(N_c+m-1)} \\ \mathbf{F}^{(m)} &= Q^{(m)}\mathbf{\Phi}_F\mu^{(m-1)} + Q^{\star(m)}\mathbf{\Phi}_F^\star\mu^{(N_c+m-1)} \end{aligned} \tag{13}$$

Where $\mathbf{\Phi}$ and $\mathbf{\Phi}^\star$ are the eigenvectors of Equation (11), and Q and $Q^\star$ are the wave amplitudes at interface m, with $m = [1, N_c + 1]$. There are $2n$ eigenvalues and eigenvectors representing the modes of wave propagation, separated into incident waves $\mu_j \leq 1$ and reflected waves $\bar{\mu}_j^\star = 1/\mu_j$, with $j = 1, 2, \ldots, n$. Similarly, their respective eigenvectors are:

$$\mathbf{\Phi}_j = \begin{Bmatrix} \mathbf{\Phi}_{uj} \\ \mathbf{\Phi}_{Fj} \end{Bmatrix}, \mathbf{\Phi}_j^\star = \begin{Bmatrix} \mathbf{\Phi^\star}_{uj} \\ \mathbf{\Phi^\star}_{Fj} \end{Bmatrix} \tag{14}$$

By applying the Neumann and Dirichlet boundary conditions, the wave amplitudes can be obtained based on the boundary conditions.

$$\begin{bmatrix} Q \\ Q^\star \end{bmatrix} = \begin{bmatrix} \mathbf{I}_n & \mathbf{\Phi}_F^{-1}\mathbf{\Phi}_F^\star\mu^{(N_c)} \\ \mathbf{\Phi}_u^{\star-1}\mathbf{\Phi}_u\mu^{(N_c)} & \mathbf{I}_n \end{bmatrix}^{-1} \begin{Bmatrix} -\mathbf{\Phi}_F^{-1}\mathbf{F}_0 \\ \mathbf{\Phi}_u^{\star-1}\mathbf{u}_o \end{Bmatrix} \tag{15}$$

Where $\mathbf{F}_0$ and $\mathbf{u}_0$ are the boundary conditions of the structure.

2.3 Spectral Element Method for frames

The spectral element model of the frame ($\mathbf{S_f}$) is obtained by combining the spectral elements of rods and beams to form the spectral dynamic stiffness matrix. Authors such as (Lee, 2009; Doyle, 1997) have explored this method, which is based on solving the partial differential equations of each element. The spectral dynamic stiffness matrix of the beam ($\mathbf{S_B}$) is given by (Lee, 2009):

$$\mathbf{S_B}(\omega) = \frac{EI_z}{L^3} = \begin{bmatrix} S_{B11} & S_{B12} & S_{B13} & S_{B14} \\ S_{B12} & S_{B22} & S_{B23} & S_{B24} \\ S_{B13} & S_{B23} & S_{B33} & S_{B34} \\ S_{B14} & S_{B24} & S_{B34} & S_{B44} \end{bmatrix} \tag{16}$$

Where,

$$S_{B11} = S_{B33} = \Delta_B \bar{L}^3(\cos\bar{L}\sinh\bar{L} + \sinh\bar{L}\cosh\bar{L})$$
$$S_{B22} = S_{B44} = \Delta_B \bar{L}^3 k_B^{-2}(-\cos\bar{L}\sinh\bar{L} + \sinh\bar{L}\cosh\bar{L})$$
$$S_{B12} = -S_{B34} = \Delta_B \bar{L}^3 k_B^{-1}\sin\bar{L}\sinh\bar{L})$$
$$S_{B13} = -\Delta_B \bar{L}^3(\sin\bar{L} + \sinh\bar{L})$$
$$S_{B14} = -S_{B23} = \Delta_B \bar{L}^3 k_B^{-1}(-\cos\bar{L} + \cosh\bar{L})$$
$$S_{B24} = \Delta_B \bar{L}^3 k_B^{-2}(-\sin\bar{L} + \sinh\bar{L}$$
$$\Delta_B = \frac{1}{1 - \cos\bar{L} + \sinh\bar{L}}$$
$$\bar{L} = k_B L$$
$$k_B(\omega) = \sqrt{\omega}\left(\frac{\rho A}{E I_Z}\right)^{\frac{1}{4}}$$

Where k_B is the wave number of the beam element. The spectral dynamic stiffness matrix of the rod ($\mathbf{S_R}$) is defined as follows (Lee, 2009) :

$$\mathbf{S_R}(\omega) = \frac{EA}{L}\begin{bmatrix} S_{R11} & S_{R12} \\ S_{R12} & S_{R22} \end{bmatrix} \tag{17}$$

Where,

$$S_{R11} = S_{R22} = (k_R L)\cot(k_R L)$$
$$S_{R12} = -(k_R L)\csc(k_R L)$$
$$k_R(\omega) = \omega\sqrt{\frac{\rho}{E}}$$

Where k_R is the wave number of the rod element. Finally, the spectral dynamic stiffness matrix of the frame is obtained by combining equations (16) and (17).

$$\mathbf{S_f} = \begin{bmatrix} \mathbf{S_R}(1,1) & 0 & 0 & \mathbf{S_R}(1,2) & 0 & 0 \\ 0 & \mathbf{S_B}(1,1) & \mathbf{S_B}(1,2) & 0 & \mathbf{S_B}(1,3) & \mathbf{S_B}(1,4) \\ 0 & \mathbf{S_B}(2,1) & \mathbf{S_B}(2,2) & 0 & \mathbf{S_B}(2,3) & \mathbf{S_B}(2,4) \\ \mathbf{S_R}(2,1) & 0 & 0 & \mathbf{S_R}(2,2) & 0 & 0 \\ 0 & \mathbf{S_B}(3,1) & \mathbf{S_B}(3,2) & 0 & \mathbf{S_B}(3,3) & \mathbf{S_B}(3,4) \\ 0 & \mathbf{S_B}(4,1) & \mathbf{S_B}(4,2) & 0 & \mathbf{S_B}(4,3) & \mathbf{S_B}(4,4) \end{bmatrix} \tag{18}$$

To transform from the local coordinate system to the global coordinate system, the rotation matrix given by Eq. (3) is used as follows:

$$\mathbf{S} = \mathbf{\Psi}^T \mathbf{S_f} \mathbf{\Psi} \tag{19}$$

The equation of dynamic equilibrium remains the same as in the FEM, given by Eq. (6), and the dynamic matrix of the resonators is given by Eq. (8), which takes into account that the resonators are in the degree of freedom of the transverse displacement at the junction node of each material.

3. RESULTS AND DISCUSSION

The presented methods are used for the proposed structure, where numerical simulations are performed. Tab. 1 presents the structural geometric parameters and material properties used in the simulation.

To validate the calculated results, the transmittance between the points Q and the applied force were calculated using the FEM, WFE, and SEM methods. Fig. 5 shows the transmittance and dispersion diagram of a 6x2 structure, where all three methods converge to the same result. The properties of the structure are described in Tab. 1, with a structural damping coefficient of $\eta = 0.01$ and a free-free boundary condition, a force of $F_o = 1$ N is applied.

Figure 5a shows the attenuations caused by the local resonance effect between 1100 Hz and 1600 Hz in the first gray region, due to the coupled local resonators in the structure. For the subsequent three highlighted regions, the destructive Bragg effect can be observed, which is generated by the impedance mismatch created by the composition of the phononic crystal. Fig. 5b displays the dispersion diagram, composed of a real part (red) and an imaginary part (blue). The dispersion diagram is obtained from the wave number in Eq. (12) and illustrates the wave propagation in a structure with an infinite number of cells. The real part represents the propagating waves, while the imaginary part represents the evanescent waves.

Table 1: Structural Parameters and Material Properties.

Geometry/Property	**Value**
Steel density (kg/m^3)	7800
Steel Young's module (Pa)	$210 \cdot 10^9$
Polyacetal density (kg/m^3)	1140
Polyacetal Young's module (Pa)	$2.41 \cdot 10^9$
Cross-sectional area (m^2)	$8 \cdot 10^{-4}$
Beam Length (m)	0.3
Steel beam length (m)	0.09
Polyacetal beam length (m)	0.12
L (beam length) (m)	0.3
β (polyacetal composition %)	40

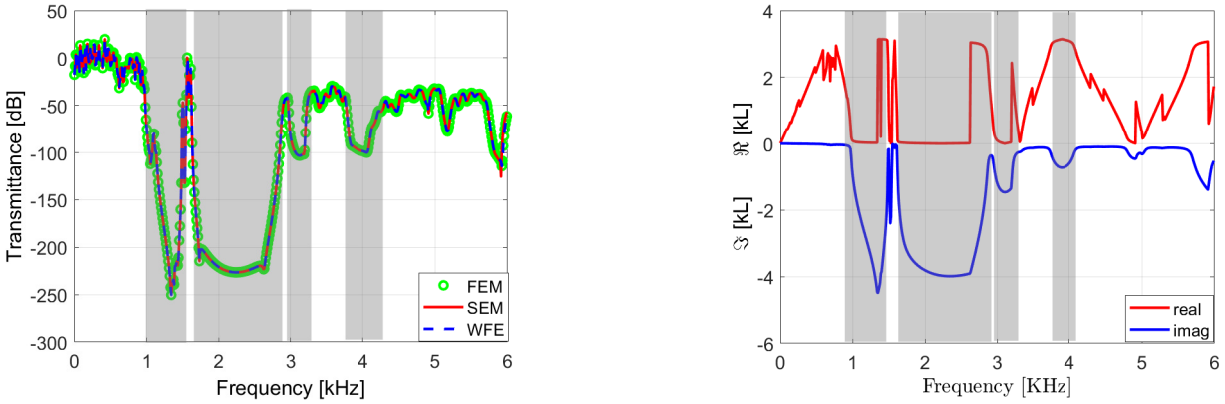

(a) Transmittance. (b) Dispersion diagram.

Figure 5: Transmittance and dispersion diagram for a 6 x 2 structure. The spring stiffness is $k_r = 1 \times 10^7$ Pa and $m_r = 0.1233$ kg, and the resonator's natural frequency is 1433.5 Hz.

The bandgaps occur when the real part is equal to zero or π (Bragg limit). In this structure, the four formed bandgaps are represented in the frequency ranges of attenuation in the forced response. The attenuations caused by the Bragg effect due to the composition of the phononic crystal in the structure occur at frequencies above 1000 Hz. The coupling of a local resonator in the structure allows for the control of vibrations at frequencies below 1 kHz. Fig. 6 presents a comparison between the forced responses of the structure with and without the resonator. The highlighted region in Fig.6a illustrates the attenuation caused by the local resonance of the coupled resonator, between 700 Hz and 1050 Hz. In this frequency range, the control is mainly influenced by the mass of the resonator, as described in Eq. (8). Fig. 6b displays the dispersion diagram with the highlighted bandgap region of the resonator.

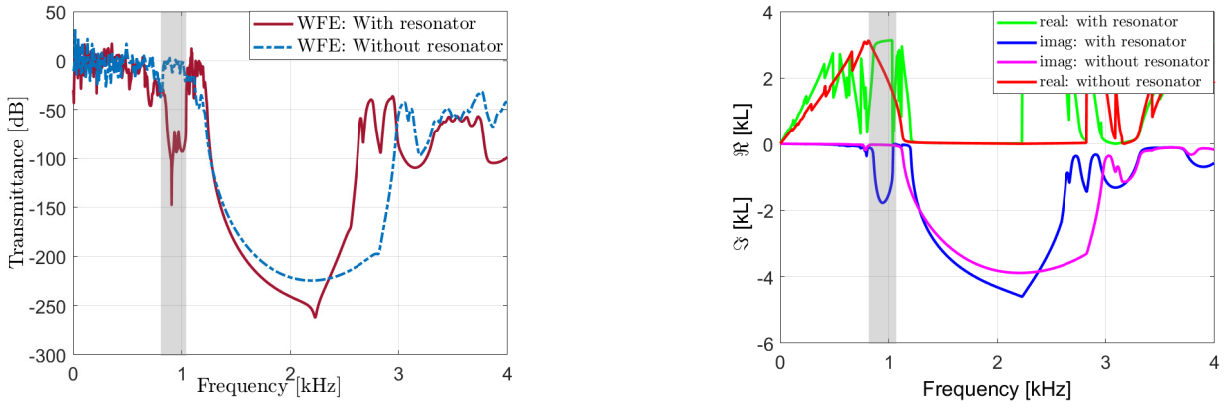

(a) Transmittance. (b) Dispersion diagram

Figure 6: Transmittance and dispersion diagram for a 6x2 structure with and without local resonators. The spring stiffness is $k_r = 1 \times 10^7$ Pa and the mass of the resonator is $m_r = 0.3082$ kg, with a natural resonant frequency of 906.63 Hz.

Figure 7 presents the results of the WFE method for the attenuations near the resonant frequencies of the resonator, as a function of its mass, which was varied from 5% to 25% of the mass of each Euler-Bernoulli beam. These results are consistent with other authors, such as (Xiao *et al.*, 2013; Zhang *et al.*, 2019). The attenuations occur due to the interaction between the added mass and the vibrational properties of the resonator. Increasing the mass causes a shift in the resonant frequency, resulting in different levels and frequency ranges of attenuation. This enables greater vibrational control at lower frequencies.

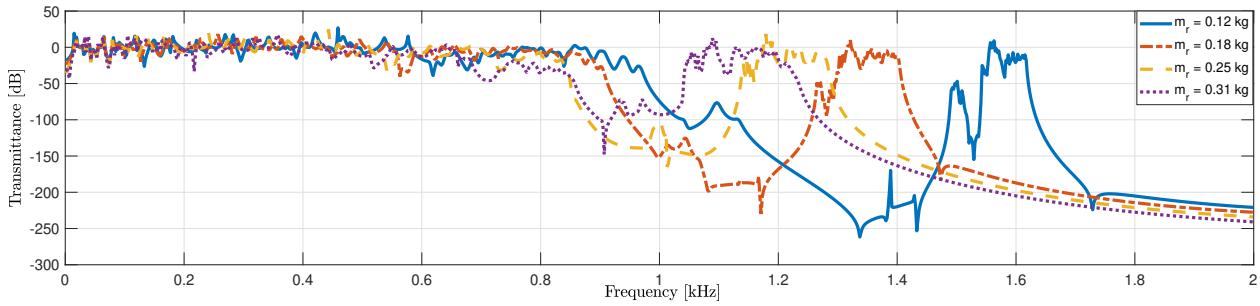

Figure 7: Transmittance for a 6 x 2 structure. The spring stiffness is $k_r = 1 \times 10^7$ Pa. The resonant frequencies of each resonator, respectively : 1434 Hz, 1170 Hz, 1014 Hz, and 906 Hz.

Figure 8 shows two structural parametric variations obtained using the WFE method. In Figure 8a, there is a variation in the composition of polycetal in each Euler-Bernoulli beam, ranging from 10% to 60%, while the mass of the resonator is kept at 10% of the beam's mass. It can be observed that for compositions below 25% of polycetal, the resonator does not have a significant effect, and the Bragg effect occurs only at high frequencies. With an increase in the polycetal composition (β), local resonance arises at lower frequencies, and the attenuation band widens. Additionally, the Bragg effect, caused by the impedance difference in the structure, emerges at frequencies between 2 kHz and 3 kHz.

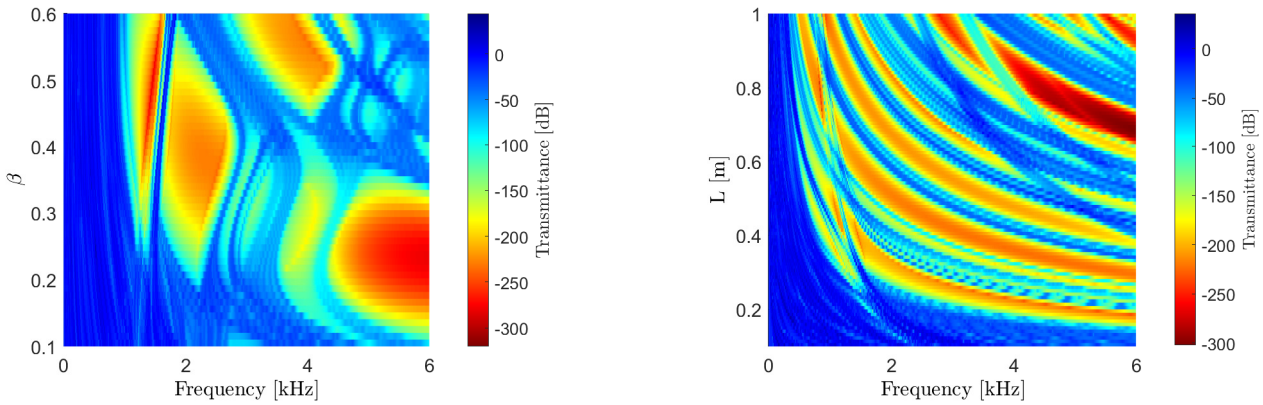

(a) Variation in material composition.

(b) Variation in the length of the Euler-Bernoulli beam.

Figure 8: Transmittance for a 6 x 2 structure. The spring stiffness is $k_r = 1 \times 10^7$ Pa..

For the variation of the length of the Euler-Bernoulli beam between 0.1 m and 1 m, with $\beta = 40\%$ and the mass of the resonator at 10% of the mass of the beam, Fig. 8b shows that the local resonance occurs above 0.25 m in the frequency range between 1.0 kHz and 1.8 kHz. These local resonances add to the first attenuation region of the Bragg effect, providing attenuation in the frequency range between 1.8 kHz and 6.0 kHz.

4. CONCLUSION

This work presented a metastructure composed of different materials, forming a phononic crystal with local resonator coupling. The FEM, WFE, and SEM methods were implemented, and the results obtained demonstrated convergence among them, indicating that the structure can be analyzed using any of these methods.

The results identified the frequencies of bandgaps in the dispersion diagram and attenuation in the transmitance, formed by the effect of the resonator and the Bragg effect. The Bragg effect occurs at higher frequencies, while the local resonators assist in vibration control at lower frequencies. The width of the attenuation band can be controlled through the mass of the resonators.

For the proposed standard structure, it was found that compositions above 25% of polyacetal in the Euler-Bernoulli

beam exhibit a local resonance effect. Furthermore, it was observed that with the increase in the structure's length, the effect of the resonators acts in conjunction with the Bragg effect, expanding the attenuation range.

5. ACKNOWLEDGEMENTS

The authors are grateful to the Brazilian research funding, FAPESP (Grant No. 15894-0/2018), CNPq (Grant No. 317436/2021-0) and FAPEMA (Grant No. BM-01652/23, APP-09180/22) for the financial support.

6. REFERENCES

Doyle, J., 1997. *Wave Propagation in Structures : Spectral Analysis Using Fast Discrete Fourier Transforms*. Springer New York, New York, NY. ISBN 9781461218326.

Goto, A.M., Nóbrega, E.D., Pereira, F.N. and Dos Santos, J.M.C., 2020. "Numerical and experimental investigation of phononic crystals via wave-based higher-order rod models". *International Journal of Mechanical Sciences*, Vol. 181, p. 105776. doi:10.1016/j.ijmecsci.2020.105776.

Hussein, M.I., Leamy, M.J. and Ruzzene, M., 2014. "Dynamics of phononic materials and structures: Historical origins, recent progress, and future outlook". *Applied Mechanics Reviews*, Vol. 66, No. 4. doi:10.1115/1.4026911.

Lee, U., 2009. *Spectral Element Method in Structural Dynamics*. John Wiley & Sons. ISBN 9780470823750.

Mead, D., 1970. "Free wave propagation in periodically supported, infinite beams". *Journal of Sound and Vibration*, Vol. 11, No. 2, pp. 181–197. ISSN 0022-460X. doi:https://doi.org/10.1016/S0022-460X(70)80062-1.

Mencik, J.M., 2008. *Approche numèrique pour la propagation multi-modale guidèe*. Ph.D. thesis.

Miranda Jr., E.J.P. and Dos Santos, J.M.C., 2018. "Flexural wave band gaps in phononic crystal euler-bernoulli beams using wave finite element and plane wave expansion methods". *Materials Research*, Vol. 20, No. suppl 2, pp. 729–742. doi:10.1590/1980-5373-mr-2016-0877.

M.Petyt, 2010. *Introduction to finite element vibration analysis*. Cambridge University Press, 2nd edition. ISBN 978-0-521-19160-9.

Nanda, A. and Karami, M., 2018. "Tunable bandgaps in a deployable metamaterial". *Journal of Sound and Vibration*, Vol. 424, pp. 120–136. ISSN 0022-460X. doi:https://doi.org/10.1016/j.jsv.2018.03.015.

Xiao, Y., Wen, J., Wang, G. and Wen, X., 2013. "Theoretical and experimental study of locally resonant and bragg band gaps in flexural beams carrying periodic arrays of beam-like resonators". *Journal of Vibration and Acoustics*, Vol. 135, p. 041006. doi:10.1115/1.4024214.

Zhang, Z., Li, T., Wang, Z. and Tang, Y., 2019. "Band gap characteristics of flexural wave of two-dimensional periodic frame structure composed of locally resonant composite beam". *Mechanical Systems and Signal Processing*, Vol. 131, p. 364–380.

Zhong, W. and Williams, F., 1995. "On the direct solution of wave propagation for repetitive structures". *Journal of Sound and Vibration*, Vol. 181, No. 3, pp. 485–501. ISSN 0022-460X. doi:https://doi.org/10.1006/jsvi.1995.0153.

Zuo, S., Li, F.M. and Zhang, C., 2016. "Numerical and experimental investigations on the vibration band-gap properties of periodic rigid frame structures". *Acta Mechanica*, Vol. 227. doi:10.1007/s00707-016-1587-4.

7. RESPONSIBILITY NOTICE

The authors are solely responsible for the printed material included in this paper.